Available online at www.sciencedirect.com
SCIENCE DIRECT®
International Journal of Heat and Mass Transfer 48 (2005) 5112–5120
International Journal of HEAT and MASS TRANSFER
www.elsevier.com/locate/ijhmt

One-dimensional heat transfer analysis in open-cell 10-ppi metal foam

Nihad Dukhan [a,*], Pablo D. Quiñones-Ramos [b], Edmundo Cruz-Ruiz [c], Miguel Vélez-Reyes [c], Elaine P. Scott [d]

[a] Department of Mechanical Engineering, University of Detroit Mercy, 4001 W. McNichols Rd., Detroit, MI 48221, USA
[b] University of Michigan, Ann Arbor, MI 48109, USA
[c] University of Puerto Rico-Mayagüez, Mayagüez, PR 00680, USA
[d] Virginia Polytechnic and State University, Blacksburg, VA 24061, USA

Received 30 July 2004; received in revised form 30 July 2005
Available online 26 September 2005

Abstract

A one-dimensional heat transfer model for open-cell metal foam is presented. The model combines the conduction in the ligaments and the convection to the coolant in the pores. The approach avoids a complete three-dimensional modeling of the complex flow and heat transfer inside the foam. The temperature along the foam decayed exponentially with the distance from the heated base. The model and the one-dimensional assumption were verified by direct experiment on a thin aluminum foam sample of ten pores per inch for a range of pore Reynolds number. Good agreement was found between the analytical and the experimental results.

Keywords: Convection; Heat transfer; Porous media; Metal foam

1. Introduction

Metal foams are a relatively new class of materials with low densities and novel thermal, mechanical, electrical and acoustic properties. They offer a great potential for significant performance gains. Their use and applications have been widening. For example, metal foams have been used as lightweight supporting structure in aerospace applications [1,2]. Different types of metal foams are used as a buffer between a stiff structure and a fluctuating temperature field. They are also used in geothermal operations and in petroleum reservoirs [3]. Ceramic foams are used in advanced burners and heat pipes. And nickel foams have been used in high-power batteries for lightweight cordless electronics [2]. Thermal management applications of foams include compact heat exchangers for airborne equipment, air-cooled condenser towers and compact heat sinks for power electronics [1]. The open porosity, low relative density and high thermal conductivity of the cell edges, the large accessible surface area per unit volume, and the ability to mix the cooling fluid by promoting eddies [4], all make metal foam heat exchangers efficient, compact and light weight.

Current models for packed beds are not exactly applicable to high porosity metal foam [3]. Packed beds

* Corresponding author. Tel.: +1 313 993 1579; fax: +1 313 993 1187.
E-mail address: ndukhan@att.net (N. Dukhan).

0017-9310/$ - see front matter © 2005 Elsevier Ltd. All rights reserved.
doi:10.1016/j.ijheatmasstransfer.2005.07.012

Nomenclature

A	area
d	ligament diameter
h	convection heat transfer coefficient
k	thermal conductivity
L	length of foam sample
m	fin parameter
Nu	Nusselt number in foam
P	perimeter of foam sample
ppi	number of pores per inch
Pr	Prandtl number
q	heat transfer
Re	pore Reynolds number
T	temperature
t	thickness of foam sample
U	approach velocity
u	pore velocity
W	width of fin or foam sample
x	axial coordinate along foam sample
X	nondimensional distance along foam sample
y	coordinate along width foam sample
z	coordinate along direction of flow

Greek symbols

ε	porosity
θ	dimensionless temperature
λ	correction factor for Nu
ν	kinematic viscosity
ρ	relative density of foam
σ	surface area per unit volume of foam

Subscripts

b	at the base ($x = 0$)
c	cross-sectional
condf	conduction in fluid
conds	conduction in solid
conv	convection
eff	effective value
f	fluid
fm	foam
p	pore
s	solid
x	axial direction
∞	ambient

and granular media in general have a porosity ranging from 0.3 to 0.6, while high porosity metal foams have porosities greater than 0.9 [5].

The porous matrix consists of tortuous, irregularly shaped flow passages. Heat transfer takes place between the surface of the solid matrix and the fluid. The flow recirculates at the back of the solid fibers, and for pore-scale Reynolds number greater than 100, turbulence and unsteady flows occur [6]. The geometric complexity and the random orientation of the solid phase of the porous medium prevent exact solutions of the transport equations inside the pores [3,7,8]. Empirical treatments, on the other hand, require the determination of one or more parameters experimentally. Moreover, there are disagreements among researchers regarding the heat transfer correlations and the characteristic length to be used [9].

Due to their novelty and peculiar structure, metal foams are still incompletely characterized. Although the knowledge base is improving with time, the recent upsurge of utilizing high porosity media in contemporary technologies makes the need for fully characterizing them more urgent. In terms of heat transfer, simple reliable models of the heat transfer for foam would certainly help the engineering research community.

A number of studies were undertaken to fill this information gap. Decker et al. [7] provided detailed experimental characterization and numerical modeling of the heat and mass transport properties of highly porous media for solar receivers and porous burners. They considered the foam as a pseudo-homogeneous (locally-volume-averaged) medium, where the solid and the fluid phases were treated as an artificial single phase with effective properties.

Many researchers focused on determining the effective thermal conductivity. Bhattacharya et al. [5], for example, provided analytical and experimental results for the effective thermal conductivity for high porosity metal foams. The analytical model represented the foam by a two-dimensional array of hexagonal cells. The porosity and the pore density were used to describe the porous media.

Pan et al. [10] experimentally determined the effective thermal conductivities of foams made out of aluminum and silicon alloys. Writz [11] presented a semi-empirical model for the combined conduction and convection heat transfer in a thin porous wall. The model assumed a one-dimensional conduction in the porous matrix and a one-dimensional flow of the coolant through the foam wall. For the same volume of the heat exchanger, the porous matrix provided approximately 1.5 times more heat transfer surface than the offset strip fin array.

Kumar and Murthy [12] developed an unstructured finite-volume numerical technique for computing the effective thermal conductivity of complex porous media. The porous media was made from random beds of spheres and rods separately. For the same volume fraction of the solid, the distribution of the solid phase in the porous media had a strong effect on the effective conductivity.

Other researches were interested in the metal foam as heat sinks. Bastawros [4], for example, provided experimental measurements and modeling of the thermal and hydraulic aspects of cellular metals subject to transverse airflow. Results showed that at low velocities, the heat flux was governed by the convective heat transfer to the flowing fluid. At higher velocities, the heat flux was limited by the heat conduction from the substrate to the foam block through the constricted nodal passages of the foam. With specific regard to cellular metals, Bastawros et al. [6] characterized the foam morphology based on the cell ligament diameter and the relative density.

Kim et al. [13] numerically investigated the anisotropy in permeability and effective thermal conductivity on the performance of an aluminum heat sink. Local thermal equilibrium between the fluid and the solid in the foam was assumed. They showed that the anisotropy in permeability and effective thermal conductivity had a strong impact on the heat transfer rate.

The present work provides a macroscopic lumped-parameter engineering treatment to determine the temperature distribution in open-cell metal foams when they are used in a forced convective heat transfer mode. The analysis uses the typical parameters reported by the foam manufacturers such as the porosity and the area density, defined as the ratio of the surface area of the foam to the volume. The simplicity and applicability of the present approach offer a significant advantage over previous treatments: It eliminates the need for rigorous microscopic analytical or numerical modeling of the flow and the heat transfer in and around the pores. Another advantage is that the current model is easily verified by simple experiments, as described below. Even though the model is derived for a thin foam sample, it may be applicable to other shapes of foams. This extrapolation is expected because other researchers [2,14] have shown that effective thermal properties, such as the conductivity, were independent of the thickness of the foam sample.

2. Heat transfer model

The current analysis seeks to develop closed form results for a rectangular block of thin porous foam having a constant cross-sectional area by treating it as an extended fin. Let the block have a length L, width W and thickness t as shown in Fig. 1. Let the temperature at the base of the foam be T_b. Let a coolant flow through the porous foam by directing it perpendicularly to one of the foam's surfaces as shown in Fig. 1. This condition gives rise to forced convection heat transfer inside the pores of the foam. The heat transfer coefficient for this convection, h_{fm}, is available from previous studies [4,8]. Due to the vastly different geometry and flow field,

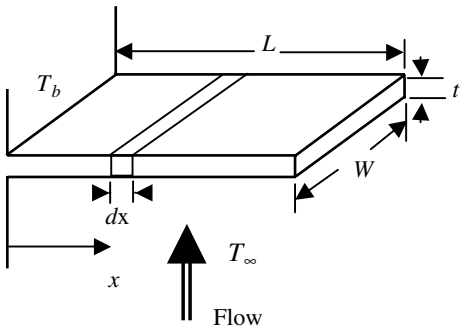

Fig. 1. Schematic and nomenclature of a constant cross-sectional-area foam sample.

h_{fm} is different from the common heat transfer coefficient for the internal or external flows on solid surfaces, and will be discussed later.

Consider now a control volume of thickness dx in the x-direction, as shown in Fig. 2. Applying conservation of energy for steady-state conditions to this control volume, we obtain

$$q_x = q_{x+dx} + q_{conv} \tag{1}$$

Radiation heat transfer is neglected and is assumed to be small for applications in which the temperature reaches only moderate levels. The ratio of radiation to the total heat transfer is between 0.5% and 4% [10]. The conduction terms are readily given by Fourier's law; the convection term by Newton's law of cooling. Substituting in Eq. (1):

$$\begin{aligned} &-k_s A_{conds}\left.\frac{dT_{fm}}{dx}\right|_x - k_f A_{condf}\left.\frac{dT_{fm}}{dx}\right|_x \\ &\quad = -k_s A_{cond}\left.\frac{dT_{fm}}{dx}\right|_{x+dx} - k_f A_{condf}\left.\frac{dT_{fm}}{dx}\right|_{x+dx} \\ &\qquad + h_{fm} A_{conv}(T_{fm} - T_\infty) \end{aligned} \tag{2}$$

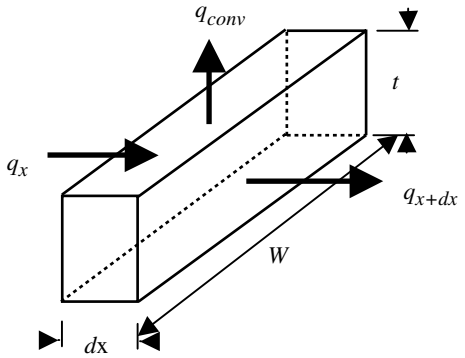

Fig. 2. Control volume for the foam.

The areas for conduction in the ligaments and in the coolant depend on the porosity, ε, and were approximated by Sullines and Daryabeige [2]:

$$A_{\text{conds}} = A_{\text{c}} - A_{\text{p}} = A_{\text{c}}(1-\varepsilon) \tag{3}$$

and

$$A_{\text{condf}} = A_{\text{p}} = A_{\text{c}}\varepsilon \tag{4}$$

where A_{c} is the cross-sectional area and A_{p} is the area occupied by the pores, i.e., the coolant not the solid material of the foam. The porosity is a property that can be easily measured, or is reported by the foam manufacturers. It is defined as the volume of the solid phase divided by the total volume of the foam. For the control volume of Fig. 2, the area for convection is simply given by

$$A_{\text{conv}} = \sigma \cdot A_{\text{c}}\,\mathrm{d}x \tag{5}$$

where σ is the surface area per unit volume, which is also a property usually reported by the foam manufacturers. Substituting for the heat transfer areas, simplifying and rearranging, Eq. (2) becomes

$$\frac{\mathrm{d}^2 T_{\text{fm}}}{\mathrm{d}x^2} - \frac{h_{\text{fm}}\sigma}{k_{\text{s}}(1-\varepsilon)+k_{\text{f}}\varepsilon}(T_{\text{fm}} - T_{\infty}) = 0 \tag{6}$$

or

$$\frac{\mathrm{d}^2\theta}{\mathrm{d}X^2} - m_{\text{fm}}^2\theta = 0 \tag{7}$$

where $\theta = \frac{T_{\text{fm}}-T_{\infty}}{T_{\text{b}}-T_{\infty}}$, $X = \frac{x}{L}$ and m_{fm} is a new parameter named the "foam parameter" given by

$$m_{\text{fm}}^2 = \frac{h_{\text{fm}}\sigma L^2}{k_{\text{s}}(1-\varepsilon)+k_{\text{f}}\varepsilon} \tag{8}$$

The boundary conditions for Eq. (7) are

1. $X = 0$, $\theta = 1$.
2. $X = 1$, $\mathrm{d}\theta/\mathrm{d}X = 0$.

The first boundary condition says that the temperature at the boundary of the foam is the same as the ambient, while the other says that at the exit of the foam, the temperature of the foam attains its maximum value. This is the point where no more heat addition occurs. The solution is the one-dimensional foam temperature distribution given by:

$$\theta(X) = \frac{\cosh m_{\text{fm}}(1-X)}{\cosh m_{\text{fm}}} \tag{9}$$

3. The foam average temperature assumption

The above analysis assumes that the temperature of the solid ligaments and the coolant inside the pores of the foam, at any x-location, are approximately the same. This temperature is referred to as the foam temperature. To justify this assumption, we attempted to estimate the maximum possible temperature difference between the solid ligaments and the fluid. To simplify the analysis, and to present the worst-case scenario, the random geometry of the solid ligaments, Fig. 3(a), was approximated by a bank of cylinders in cross-flow, Fig. 3(c). Simplifications like this are not uncommon. Bhattacharya et al. [5], for example, represented the foam structure by an arrangement of cubes, Fig. 3(b).

The flow field in the foam (Fig. 3(a)) certainly provides more mixing and turbulence due to its random geometry, while the cubic arrangement in Fig. 3(b) offers less mixing and turbulence. This is followed by the very simple bank of parallel cylinders (Fig. 3(c)), which offers the least amount of mixing and turbulence. Therefore, one may argue that if the solid and the fluid temperatures are close for the last case, they must be even closer in the first case. The following is an estimate of the temperature difference in the third case. The bank of cylinders is characterized by the cylinder diameter d (which is the ligament diameter of the foam), a transverse pitch S_{T} measured between cylinder centers.

Let the fluid's approach velocity be U. The pore velocity, u, in the pores of open-cell metal foam is defined by Bastawros et al. [6]:

$$u = \frac{U}{1-\rho} \tag{10}$$

where ρ is the relative density of the foam sample.

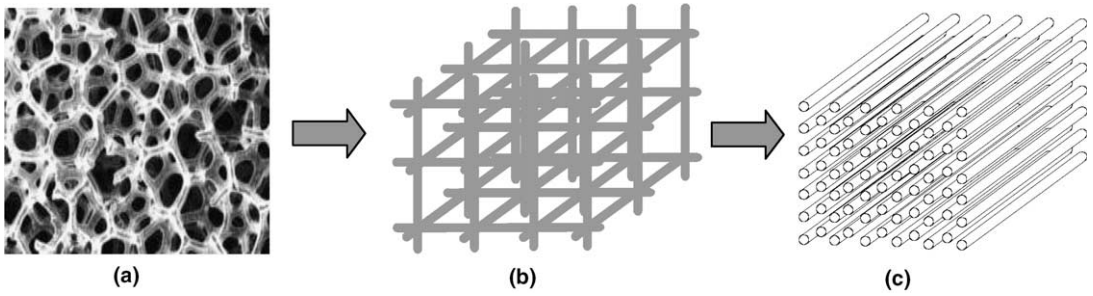

Fig. 3. Metal foam representations: (a) actual foam structure, (b) as an arrangement of cubes, (c) as a bank of cylinders.

The pore Reynolds number is

$$Re = \frac{ud}{v} \tag{11}$$

where v is the kinematic viscosity of the fluid.

Bastawros et al. [6] suggested a correction factor, λ, for the Holman correlation for a microscopic bank of cylinders in turbulent flow, to account for the geometrical difference between the foam and the bank of cylinders:

$$Nu = \frac{h_{\mathrm{fm}} d}{k_{\mathrm{f}}} = 0.62\lambda Pr^{0.36} Re^{0.5} \quad Re > 40 \tag{12}$$

where h_{fm} is the convective heat transfer coefficient inside the foam, k_{f} is the fluid thermal conductivity and Pr is the Prandtl number. The coefficient λ was determined by experimental calibration [6]: $\lambda = 0.42 \pm 0.09$.

For a bank of cylinders, Fig. 3(c), the temperature difference between the cylinder surface temperature T_{s} and the fluid leaving the bank T_{o} is [15]

$$\frac{T_{\mathrm{s}} - T_{\mathrm{o}}}{T_{\mathrm{s}} - T_{\mathrm{i}}} = \exp\left(-\frac{\pi d N h_{\mathrm{fm}}}{\rho U N_{\mathrm{T}} S_{\mathrm{T}} c_p}\right) \tag{13}$$

where T_{i} is the fluid inlet temperature (T_∞ for the foam), N is the total number of tubes, N_{T} is the number of tube rows in the transverse plane and S_{T} is the pitch.

The analysis is applied to a small portion of foam, located in the most critical zone, Fig. 4. This zone is subject to the air entering the foam and to the maximum base temperature.

The diameter of the cylinders presented in the figure is equal to the diameter of the foam ligaments. The value of this parameter is taken from Bhattacharya et al. [5] who employed a microscope to measure the ligament diameter. It was found that the ligament diameter for a 10-ppi sample is equal to 0.42 mm. To estimate the pitch, we used the pore size, which is established by the number of pores that can be counted in a distance of one inch (the ppi). Therefore, for a 10-ppi foam $S_{\mathrm{T}} = 2.54 \times 10^{-4}$ m.

The air density and the heat capacity were obtained from tables at 22 °C. The ligament surface temperature was taken as the highest base temperature observed during the experiments (44 °C). It was decided to take a length of 2.54 cm along the fluid flow direction and a height of 1.27 mm. These parameters would allow having a total of 100 cylinders arranged in five rows of in the transverse plane. This only takes into account the horizontal ligaments. To account for the vertical ligaments, we doubled the number of horizontal cylinders. This reduced the pitch to half of its original length, the total number of cylinders to 200, and increased the number of rows in the transverse plane to ten. Substituting these parameters, and the convective coefficient from Eq. (12), in Eq. (13), we obtain the temperature difference. Table 1 presents the temperature difference between the surface filament and the air at 2.54 cm from the entrance for different pore Reynolds numbers corresponding to different approach velocities U.

The difference in temperature is very small: It has a maximum of 0.21 °C at the highest pore Reynolds number. As stated earlier, the actual difference in the foam is expected to be less and thus can be ignored.

Table 1
Estimated temperature difference between the solid and the fluid at $x = 2.54$ cm

Pore Reynolds number	Temperature difference (°C)
75.7	0.01
168.3	0.09
216.6	0.16
241.2	0.21

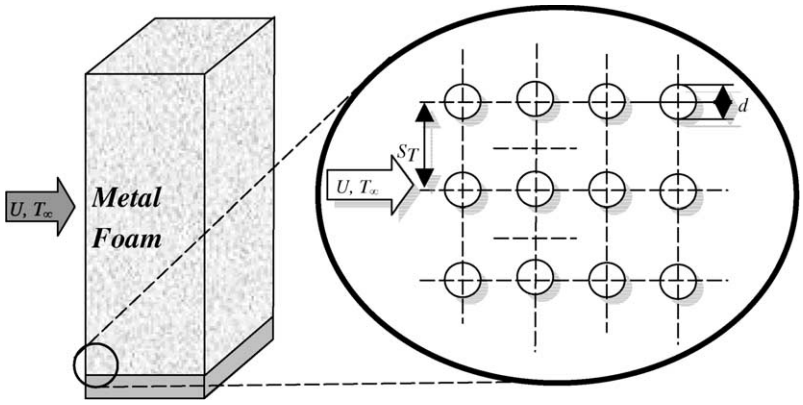

Fig. 4. Representation of foam ligaments as a bank of cylinders.

4. Experiment

In order to verify the above results, a thin sample of commercially available open-cell aluminum foam was tested. The sample was made from aluminum alloy 6101-T6 having a material density of 2700 kg/m^3. Other foam parameters were obtained from Ozmat et al. [16] and ERG Materials and Aerospace [17] and are shown in Table 2.

The dimensions of the sample were $W = 101.6$ mm, $t = 50.8$ mm and $L = 241.3$ mm. The sample was brazed to a 12.7-mm thick solid aluminum base (Fig. 5). The brazing eliminated any thermal contact resistance.

Experiments were performed in the Porous Media Research Lab of the authors' using a wind tunnel. The tunnel was an open-loop wind tunnel shown schematically in Fig. 6. Room air was forced to flow into this tunnel by a suction fan located close to its exit. The exit had a sliding plate that changed the size of the exit area, thus controlling the volumetric flow rate through the tunnel. A 5-cm thick section of flow straightener was placed close to the entrance. The size of the tunnel's test section was 14.9 cm by 30.2 cm, and had an integrated manometer for pressure measurements in mm of water.

The foam sample was provided with a thin thermfoil heater having a surface area identical to its solid aluminum base. The heater was connected to a DC power supply to provide the electrical power. The four sides of the foam sample that constituted its outer perimeter were insulated using 2.54-cm thick Styrofoam insulation, and the sample was placed in the tunnel's test section. The other two sides were perpendicular to the flow direction and remained open to the airflow. The insulation material ensured that the flow would travel through the foam only, allowing only a negligible flow between the insulation and the tunnel walls.

Table 2
Foam parameters

σ (m^2/m^3)	d (mm)	ρ	ε
804	0.419	0.082	0.918

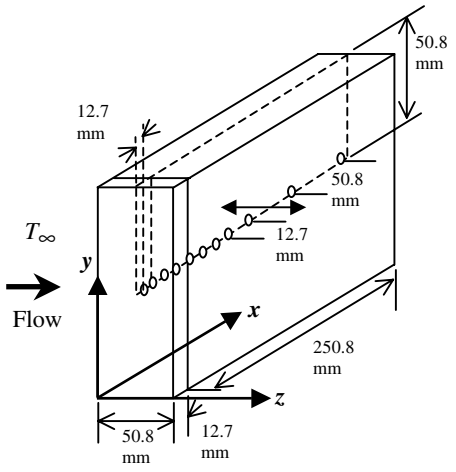

Fig. 5. Schematic of the foam sample.

A total of thirteen thermocouples were used to measure the temperature at different strategic locations in the foam as well as the ambient and the base temperatures. The temperature measurement locations in the sample are shown in Fig. 5 (the small circles) and are listed in Table 3. Smaller spacing of the thermocouples was used closer to the base, to capture the anticipated steep drop in temperature. The thermocouples were attached to the channels of an automatic data acquisition system, connected to a computer, where the temperature readings were recorded, as shown in Fig. 6. Temperature measurements tracing the direction of the flow (z-direction) at different x-locations were made according to Table 3.

The dynamic pressure of the air, after traveling through the metal foam, was measured using the manometer. This pressure was used to calculate the average velocities and actual flow rates. The results are shown in Table 4.

Temperature measurements were taken at four different flow rates of the tunnel. The temperature measurements traced the z-direction at $z = 0.64$, 1.27, 2.54, 3.81 and 4.44 cm in the plane $y = 5.08$ cm. The dependence of the temperature on the y-direction was eliminated based on the symmetry of the boundary conditions, i.e., insulation at $y = 0$ and at $y = 10.16$ cm. Actually measurements were performed for this direction to verify this assumption and are not shown in this paper.

The uncertainty in the location of the thermocouples was ± 0.8 mm. As for the temperature measurements, the calibration uncertainty was ± 0.01 °C, and so was the uncertainty associated with the data acquisition system. The uncertainty of the thermocouple was reported as ± 1.50 °C. These uncertainties combined [18] result in a total uncertainty of ± 1.5 °C.

5. Results and discussion

Fig. 7 is a plot of the one-dimensional temperature profiles for $z = 0.64$, 1.27, 2.54, 3.81 and 4.44 cm at the lowest flow rate of 4.0 m^3/min corresponding to a pore Reynolds number of 75.5. The data points for all these locations are very close to each other. This supports the one-dimensional assumption. The temperature profiles decay in an apparent exponential fashion. The temperature in the foam reaches that of the ambient at a dimensionless distance of approximately 0.37. This

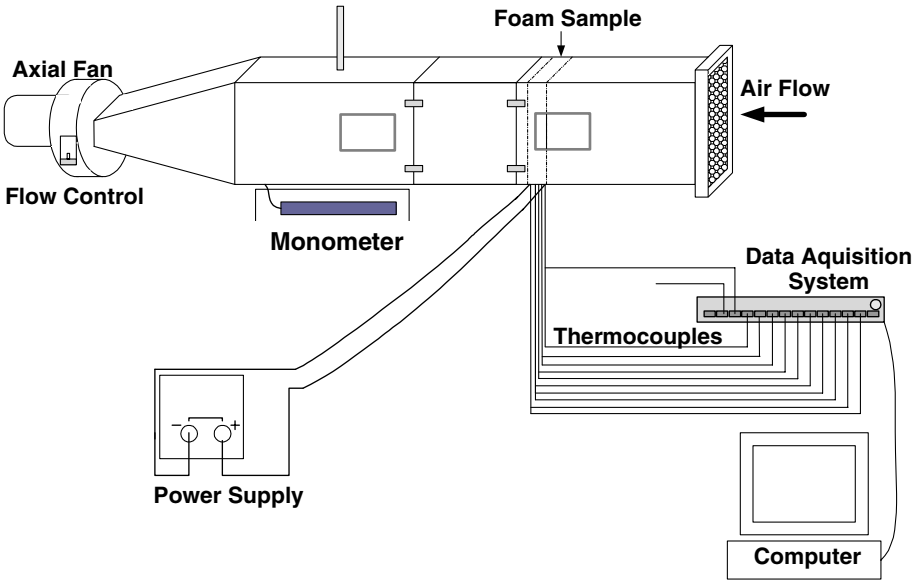

Fig. 6. Schematic of the experimental set-up.

Table 3
Thermocouple x-locations

Thermocouple no.	Location (cm)
1	0.64
2	1.27
3	1.91
4	2.54
5	3.18
6	3.81
7	4.44
8	5.08
9	6.35
10	8.89
11	13.97
12	19.05
13	Ambient

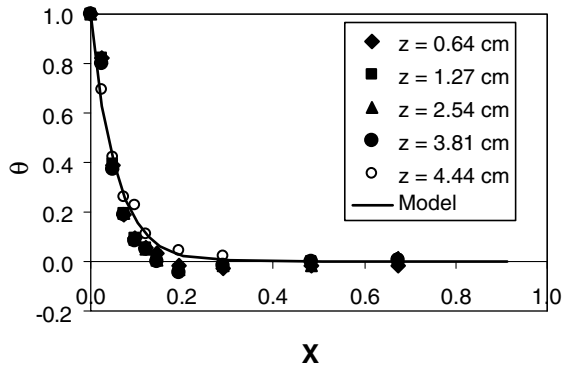

Fig. 7. Temperature distributions in the direction of the flow at $Re = 75.7$.

Table 4
Dynamic pressure measurements

Dynamic pressure (Pa)	Flow rate (m^3/min)	Pore Reynolds number
4.1	4.0	75.7
20.2	10.3	168.3
33.4	13.2	216.6
41.5	14.7	241.2

shows that most of the heat transfer takes place in a small region close to the heated base. The temperature profiles are very close to the analytical predictions given by Eq. (9) and shown by the solid line.

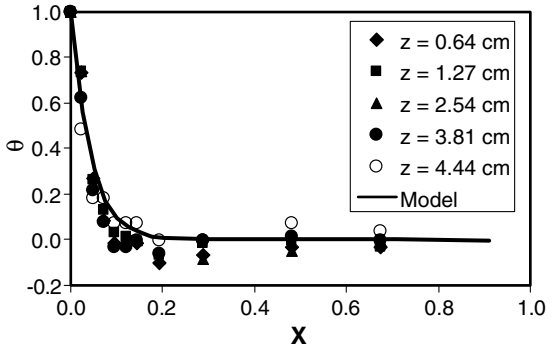

Fig. 8. Temperature distributions in the direction of the flow at $Re = 241.2$.

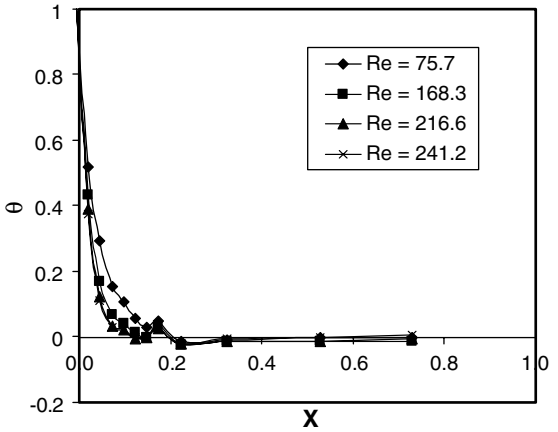

Fig. 9. Experimental temperature profiles at $z = 2.4$ cm for different Reynolds numbers.

Fig. 8 is plot of the temperature profiles for the maximum pore Reynolds number of 241.2. The same observations can be made. The experimental data points lie very close to the analytical solution shown by the solidline. The temperature in the foam drops down to the ambient temperature at an axial distance of about 0.30.

Since the model is validiated for the lowest and the highest Reynolds number, it is expected to be valid for the two intermediate values of the Reynolds number. The plots for these two cases are not shown here. The effect of the Reynolds number was obtained by measuring the x-temperature profiles at a fixed z-location of 2.54 cm at the four pore Reynolds numbers. This is shown in Fig. 9. The figure shows that the Reynolds number causes a steeper drop in the temperature profile indicating higher rate of heat transfer. This is explained as follows. Increasing the Reynolds number increase the Nusselt number or the foam heat transfer coefficient h_{fm}, as shown by Eq. (12). This increase will cause an increase in the foam parameter according to Eq. (8). This increases the argument of the hyperbolic tangent function of the temperature of Eq. (9), which causes a steeper drop. This phenomenon has a limit. It is seen that the temperature profiles for the Reynolds numbers 216.6 and 241.2 lie on top of one another. This suggests that the flow and the resulting heat transfer is independent from the Reynolds number for high enough Reynolds numbers, and there would be no increase in the heat transfer by further increasing the Reynolds number.

6. Conclusion

The combined convection and conduction heat transfer in open-cell metal foam was investigated using a one-dimensional model by treating the foam as an extended fin. The model was developed utilizing the typical parameters usually reported by the foam manufacturers. The temperature profiles were determined for one type of commercially-available aluminum foam using air as the working fluid. The model and the one-dimensional assumption were verified by direct experiment. Preliminary results showed good agreement between the model's prediction and the experimental data for a range of pore Reynolds numbers. Increasing the Reynolds number increased the heat transfer up to a certain limit.

Acknowledgements

This work was supported in part by the ERC Program of the National Science Foundation under Award Number EEC-9731677; and also by Pratt and Whitney with the help of David Cloud, for which the authors are very thankful.

References

[1] M.F. Ashby, A.G. Evans, N.A. Fleck, L.J. Gibson, J.W. Hutchinson, H.N.G. Wadley, Metal Foams, A Design Guide, Butterworth-Heinemann, Woburn, MA, 2000, pp. 181–188 (Chapter 1).
[2] D. Sullines, K. Daryabeige, Effective thermal conductivity of high porosity open cell nickel foam, in: Proceeding of the 35th AIAA Thermophysics Conference, Anaheim, CA, 2001.
[3] K. Vafai, C.L. Tien, Boundary and inertia effects on convective mass transfer in porous media, Int. J. Heat Mass Transfer 25 (8) (1982) 1183–1190.
[4] A.F. Bastawros, Effectiveness of open-cell metallic foams for high power electronic cooling, in: Proceeding, Symposium on the Thermal Management of Electronics, IMECE, Anaheim, CA, 1998.
[5] A. Bhattacharya, V.V. Calmidi, R.L. Mahajan, Thermophysical properties of high porosity metal foams, Int. J. Heat Mass Transfer 45 (2002) 1017–1031.
[6] A.F. Bastawros, A.G. Evans, H.A. Stone, Evaluation of cellular metal heat transfer media, Harvard University Report, MECH 325, 1998.
[7] S. Decker, S. Möβbauer, D.T. Nemoda, T. Zapf, Detailed Experimental Characterization and Numerical Modeling of Heat and Mass Transport Properties of Highly Porous Media for Solar Receivers and Porous Burners, Lehrstuhl für Strömungsmechanik Universität Erlangen-Nürnberg Cauerstr. 4, D-91058 Erlangen, Germany. 2000.
[8] M.L. Hunt, C.L. Tien, Effect of thermal dispersion on forced convection in fibrous media, Int. J. Heat Mass Transfer 31 (2) (1988) 301–309.
[9] L.B. Younis, R. Viskanta, Experimental determination of the volumetric heat transfer coefficient between stream of air and ceramic foam, Int. J. Heat Mass Transfer 36 (6) (1993) 1425–1434.

[10] H.L. Pan, O. Pickenacker, K. Pickenacker, D. Trimis, S. Möβbauer, K. Wawrzinek, T. Weber, Experimental Determination of the Effective Heat Conductivities of Highly Porous Media, Institute of Fluid Mechanics, University of Erlangen-Nuremberg Cauerstr. 4, D-91058 Erlangen, Germany. Available from: <www.lstm.unierlangen.de/ber2/pdf/effwl.pdf>, 2002.

[11] R.A. Writz, A semi-empirical model for porous media heat exchanger design, in: Proceedings of the American Society of Mechanical Engineers National Heat Transfer Conference, Baltimore, MD, 1997.

[12] S. Kumar, J.Y. Murthy, A numerical technique for computing effective thermal conductivity of fluid–particle mixture, Numer. Heat Transfer, Part B: Fund. 47 (6) (2005) 555–572.

[13] S.Y. Kim, J.-M. Koo, A.V. Kuznetsov, Effect of anisotropy in permeability and effective thermal conductivity on thermal performance of and aluminum foam heat sink, Numer. Heat Transfer, Part A: Appl. 40 (1) (2001) 21–36.

[14] D.A. Zumbrunnen, R. Viskanta, F.P. Incropera, Heat transfer through porous solids with complex internal geometries, Int. J. Heat Mass Transfer 29 (2) (1986) 275–284.

[15] F.P. Incropera, D.P. De Witt, Fundamentals of Heat and Mass Transfer, fifth ed., John Wiley and Sons, New York, 2002, pp. 130–133.

[16] B. Ozmat, B. Leyda, B. Benson, Applications of Open Cell Metal Foams, Personal communications with ERG Materials and Aerospace Corp., Oakland, CA, 2002.

[17] ERG Materials and Aerospace, www.ergaerospace.com, Oakland, CA, USA, 2003.

[18] R. Figliola, D. Beasly, Theory and Design for Mechanical Measurements, third ed., John Wiley and Sons, New York, 2000, pp. 124, 310.